Evolution of grain boundary network topology in 316L austenitic stainless steel during powder hot isostatic pressing

Irukuvarghula , S.; Hassanin, Hany; Cayron, C; Attallah, Moataz; Stewart, David; Preuss, Michael

Document Version
Peer reviewed version

Link to publication on Research at Birmingham portal

Evolution of grain boundary network topology in 316L austenitic stainless steel during powder hot isostatic pressing

S. Irukuvarghula [*1], H. Hassanin[2], C. Cayron[3], M. M. Attallah[4], D. Stewart[5], and M. Preuss[1]

[1]School of Materials, University of Manchester, MSS Tower, M1 3BB, UK

[2]School of Mechanical and Automotive Engineering, Kingston University, London, KT1 2EE, UK

[3]Ecole Polytechnique Fedéralé de Lausanne (EPFL), Rue de la Maladière 71b, 2000 Neuchâtel, Switzerland

[4]School of Metallurgy and Materials, University of Birmingham, Edgbaston, B15 2TT, UK

[5]Rolls-Royce, Derby, Derbyshire, DE24 8BJ, UK

Abstract

The grain boundary network evolution of 316L austenitic steel powder during its densification by hot isostatic pressing (HIPing) was investigated. While the as-received powder contained a network of random high angle grain boundaries, the fully consolidated specimen had a large fraction of annealing twins, indicating that during densification, the microstructure evolves via recrystallization. By interrupting the HIPing process at different points in time, microstructural changes were tracked quantitatively at every stage using twin boundary fractions, distribution of different types of triple junctions, and the parameters associated with twin related domains (TRDs). Results revealed that, with increase in temperature, (i) the fraction of annealing twins increased steadily, but they mostly were not part of the grain boundary network in the fully consolidated specimen and (ii) the average number of grains within a TRD, the length of longest chain, and twinning polysynthetism increased during HIPing and (iii) the powder characteristics and the HIPing parameters have a strong influence on the development of grain boundary network. Based

*Corresponding author: sandeep.irukuvarghula@manchester.ac.uk

on the results obtained, possible alterations to the HIPing process are discussed, which could potentially allow twin induced grain boundary engineering.

1   Introduction

Powder hot isostatic pressing (HIPing) is a net shape manufacturing process that is used to produce fully dense components through the application of pressure (P) and temperature (T) on a powder compact for certain amount of time (t), which results in its complete consolidation [1]. Powder HIPed components are currently being used in several industries, including oil and gas, automotive, and aerospace. HIPing is also used to remove residual porosity in castings [1]. Advantages of powder HIPing include better chemical homogeneity, fine grain size, isotropic properties, increased materials utilization, and the ability to produce complex near net shaped components. Additionally, reduced lead time for manufacturing big near net shaped components and ease of in-service inspectability are other important advantages of HIPing.

HIPing, along with other powder based manufacturing processes such as additive manufacturing, is being considered as a potential alternative for producing nuclear reactor components [2, 3]. It has been demonstrated that HIPing, owing to the advantages it offers over conventional processing, is a viable manufacturing process for producing pressure retaining components made of 316L for nuclear reactors [4, 5, 6]. 316L components produced from rolling and forging are usually used in the solution annealed, recrystallized state. Annealing twins, which are a key microstructural feature of recrystallized 316L austenitic stainless steels, are also observed in the microstructure of powder HIPed specimens (see for e.g., [7, 8]).

The presence of a large fraction of annealing twins in the fully consolidated microstructure indicates possibilities to optimize the HIPing process to enhance their fraction in the microstructure (i.e., twin induced grain boundary engineering). The importance of grain boundaries in influencing material properties has long been recognized [9, 10, 11, 12, 13]. Specifically, for face centered cubic (FCC) materials which profusely twin, previous studies have shown that twin boundaries, i.e., $\Sigma 3$ boundaries in coincidence site lattice (CSL) framework [14], are resistant towards carbide precipitation [15, 16], intergranular stress corrosion cracking (IGSCC) [17, 18, 19] and have reduced susceptibility to intergranular hydrogen embrittlement [20].

Grain boundary networks in multiple-twinned materials have previously been studied extensively within the context of grain boundary engineering and control (e.g., see [19, 21, 22, 23, 24, 25, 26, 27]). It was shown that, due to their contrasting properties,

2

the response of a material to various intergranular phenomena (e.g., intergranular stress corrosion cracking) is affected not only by the types of grain boundaries present, but also by the way they are interconnected. Since the grain boundary network topology is constrained by the crystallography at the triple junctions, it was suggested that the grain boundary connectivity, apart from quantifying the *special* boundary fraction (i.e., boundaries with CSL $\leq$ 29), can be better understood by quantifying the types of triple junctions present [28, 29, 22, 24, 25]. Specifically, based on the types of boundaries present at a triple junction (CSL and *random*), it can either allow a crack to propagate further or act as arresting point. In this approach, the response of grain boundary network towards intergranular phenomena is treated as a correlated percolation problem.

It has previously been demonstrated that in materials that are susceptible to annealing twinning, the recrystallized microstructure consists of multiple-twinned clusters called twin related domains (TRDs) [23, 30, 31, 32, 33, 34, 35]. Gertsman [23] noted that the entire microstructure is made up of TRDs and because every cluster originates from one orientation, they are linked to recrystallization. In a TRD, twinning process can proceed to any order, and thus contains twin chains. Therefore, all grains within a TRD are connected by chains of $\Sigma 3$ boundaries and are related by $\Sigma 3^n$ misorientations while the outer boundaries of TRDs have crystallographically random orientations. Since any crack propagation will only be through outer boundaries of the TRDs, they represent blocks that are generally immune to percolative phenomena and it was suggested that TRD size could be considered as the *characteristic microstructural dimension* [23, 33]. So, from the point of view of enhanced resistance towards intergranular phenomena, the microstructure must contain large TRDs with multiple twins rather than just annealing twins. Such a microstructure can be achieved by thermomechanical processing, like sequential *strain-annealing* or one-step *strain-annealing* [22, 36, 37].

Reed [30, 38] and Cayron [31, 33] developed the theory for quantifying multiple twins and identifying TRDs, while Cayron [33] suggested more advanced parameters to quantify multiple twinning, like the averages of number of grains per TRD ($\langle N_g \rangle$), length of longest chain ($\langle LLC \rangle$), polysynthetism ($\langle p \rangle$), and twinning anisotropy ($\langle a \rangle$). For a reconstructed TRD, LLC refers to the largest misorientation between two grains, and is represented by n in $\Sigma 3^n$ notation. (in other words, it represents twinning order of the TRD). Polysynthetism quantifies how frequently the individual orientations occur in a TRD. Detailed theory and the procedure for identifying TRDs have previously been reported [30, 31, 33].

Considering the importance of grain boundaries/grain boundary network in influencing the material performance, an improved understanding of the HIPing process from the standpoint of grain boundary control assumes practical significance. It is, therefore, important to identify the mechanisms/process variables that influence the microstructural

3

development during HIPing, so that they can be controlled (e.g., by altering the HIPing cycle) to produce a desired network of grain boundaries.

Hence, the objective of the present study is two fold. First, to understand the grain boundary network evolution in 316L during HIPing and identify the mechanisms/process variables that influence it. Second, since 316L can be subjected to twin induced grain boundary engineering using thermomechanical processing, and recognizing the fact that HIPing is one such process, to explore possibilities of performing grain boundary engineering during HIPing. So, the data analysis was oriented towards understanding the grain boundary network evolution and quantification of multiple twinning during HIPing. Analysis was performed on specimens that were produced by interrupting the standard HIPing cycle at various stages. In other words, evolutionary microstructural states during HIPing were captured for the analysis.

2 Materials and methods

2.1 Experimental

HIP specimens were produced from nitrogen atomised 316L powder with the chemical composition shown in Table 1 and with a less than 500 µm particle size and a mean size of 80 µm; the particle size distribution is shown in Fig. 1a. The HIPing process consisted of the following steps: the powder was first filled in mild steel canisters of 25 mm diameter, 30 mm height and 2 mm thickness, vibrated and vacuum degassed at room temperature. The canisters were then sealed by hot crimping the evacuation tube. The HIPing cycle consisted of simultaneous application of temperature and pressure at $5.5\,°C/min$ and depending on the peak HIPing temperature, at 0.62, 0.59, 0.56, and 0.54 MPa/min, respectively. HIPing was performed at $950\,°C$, $1000\,°C$, $1050\,°C$, and $1120\,°C$ at 103 MPa, without any hold time at those temperatures. Specifically, the HIPing cycle was interrupted by ramping down the temperature and pressure as soon as they reached the set points. A typical HIPing cycle is shown in Fig. 1b. Additionally, one canister (70 mm diameter and 200 mm height) was HIPed at $1160\,°C$, 103 MPa and held for 4 hours (i.e., to full HIP cycle). This sample was then solution annealed at $1050\,°C$ for 1 hour and water quenched. All specimens were sectioned, ground and polished using standard metallographic procedures. Final polishing was performed on a vibratory polisher using colloidal silica solution for 2 hours. Electron backscatter diffraction (EBSD) maps were acquired on a Field Emission Gun Scanning Electron Microscope (FEG SEM, model: CamScan Maxim), equipped with Aztec EBSD system and a Nordlys II camera. Data were acquired at 20 kV with 0.5 µm step size for the partially consolidated HIPed specimens and 1 µm for the fully consolidated specimen. EBSD maps from 5 randomly

138 selected regions per specimen were acquired for statistical analysis of the data.

Table 1: Chemical composition (in wt%) of 316L stainless steel powder determined using inductively coupled plasma mass spectrometry and intert gas fusion.

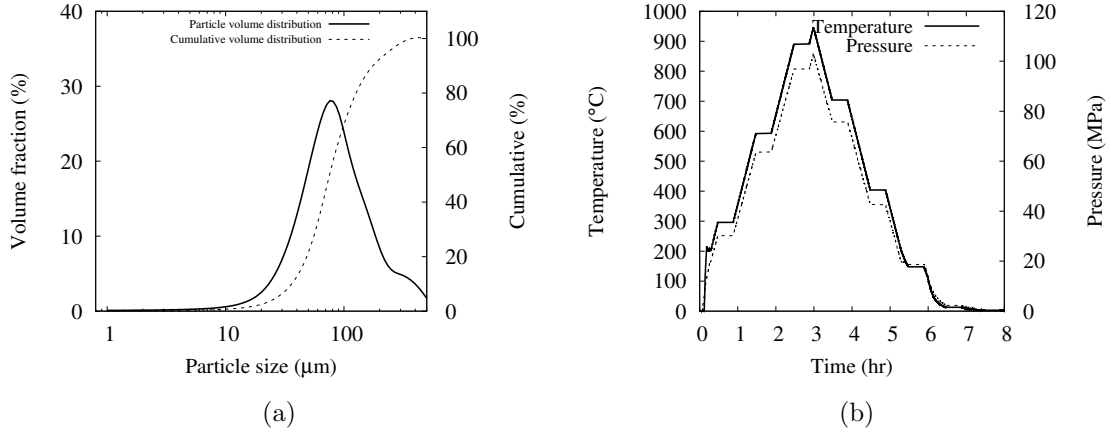| Sample	Cr	Mn	Mo	Ni	P	Si	C	S	N	O	Fe
Powder	16.44	1.32	2.08	10.14	0.023	0.57	0.018	0.002	0.098	0.02	Balance

Figure 1: (a) Particle size distribution of the powder and (b) a typical HIPing cycle used in the present study. Temperature and pressure were ramped down after reaching 950 °C and 103 MPa, respectively.

2.2   Data analysis

140 To study the evolution of grain boundary network and the microstructure of 316L powder
141 compact during its densification by HIPing, data have been analyzed by following (i)
142 the evolution of CSL boundaries and types of triple junctions and (ii) the parameters
143 associated with twin related domains. Therefore, in the present study, the fraction of
144 CSL boundaries and triple junction distributions were extracted from EBSD data using
145 MTEX, a MATLAB based open source software [39]. Boundaries with CSL ≤ 29 (with
146 a tolerance angle of $3°$ from ideal misorientation) were quantified by their length (f_{Σ}^l)
147 and number (f_{Σ}^n) fractions. It is pointed out that the quantification was performed for a
148 comparison with those published in the literature and not because all CSL boundaries $\leq$
149 29 contain special properties (except twin boundaries). Following Kumar et al [22], triple
150 junctions were classified as J_0, J_1, J_2, and J_3 where J_i constitutes a triple junction with i
151 CSL and (3-i) *random* boundaries, respectively. Only $\Sigma 3$, $\Sigma 9$, and $\Sigma 27$ boundaries were
152 considered as CSL boundaries in the triple junction analysis.

Since TRDs contain information pertaining to the microstructural development, they were analyzed in detail using ARPGE, a python based software developed by Cayron [40, 33]. A caveat needs to be mentioned regarding the experimental conditions; due to the difficulty in rapidly cooling the samples from the HIPing temperature ($\sim 5.5\,^\circ$C/min), the data reported do not necessarily correspond to the actual high temperature state of the sample. Nevertheless, the trends observed in the data from the samples HIPed at different temperatures, as will be shown below, still provide valuable information on the microstructural evolution.

3 Results

The grain boundary misorientation maps of three as-received powder particles of ~ 35 μm, 90 μm, and 225 μm size and with an average grain size of 6 μm, 10 μm, and 14 μm, respectively, are shown in Fig. 2. Here, the grain boundary misorientations are represented according to the colouring scheme proposed by Patala et al [41, 42]. This colouring scheme allows the representation of complete misorientation information (angle and axis) of the grain boundaries using the legend shown in Fig. 2e. In other words, each boundary is uniquely coloured based on its misorientation angle and axis, without broadly classifying it to be part of one category or the other (e.g., high angle and low angle, and CSL and random). For a comparison, the particle in Fig. 2c is shown with only $\Sigma3$, $\Sigma9$, and $\Sigma27$ boundaries highlighted in Fig. 2d. The rapidly solidified powders predominantly contain high angle grain boundaries, but few low angle grain boundaries are also seen (i.e., boundaries with misorientation $<5\,^\circ$, which are coloured in white in Fig. 2b). Moreover, the $\Sigma3$ grain boundaries in all particles are not long and straight, but have appearance similar to any other high angle grain boundary. In Fig. 3, a representative grain boundary misorientation map of the fully consolidated specimen is shown. It is seen that annealing twins (i.e., $\Sigma3$ boundaries in the coincidence site lattice framework [14]) form a significant fraction of the grain boundaries present in the microstructure. The appearance of parallel sided $\Sigma3$ boundaries, i.e., annealing twins, in the orientation map suggests that they had formed as a result of recrystallization during HIPing.
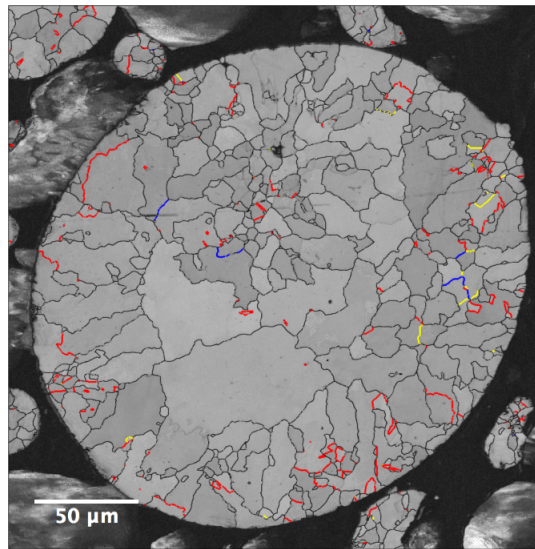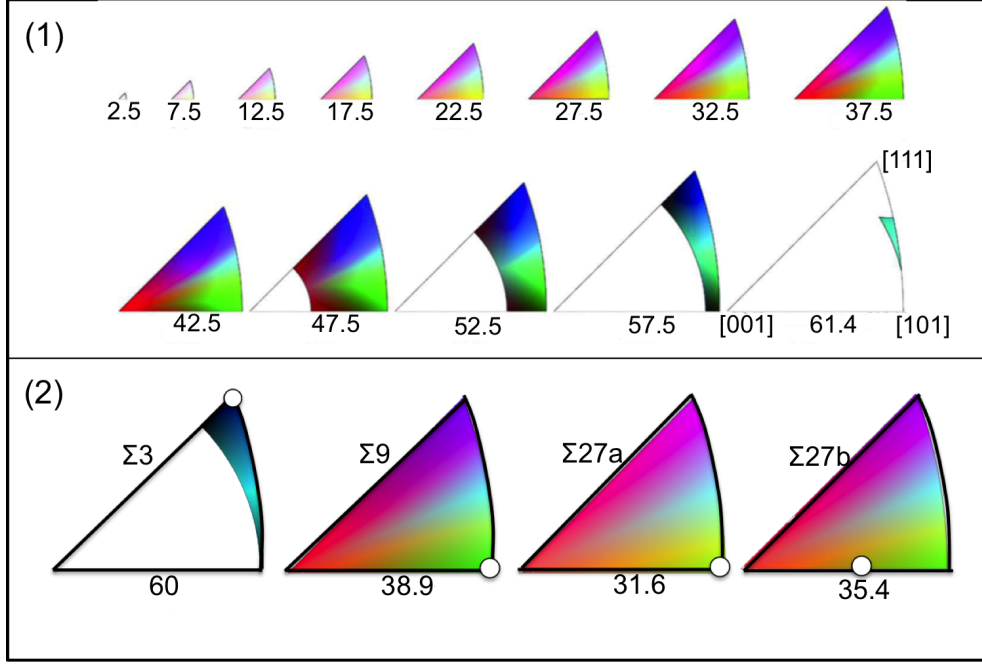
(a)

(b)

(c)

(d)
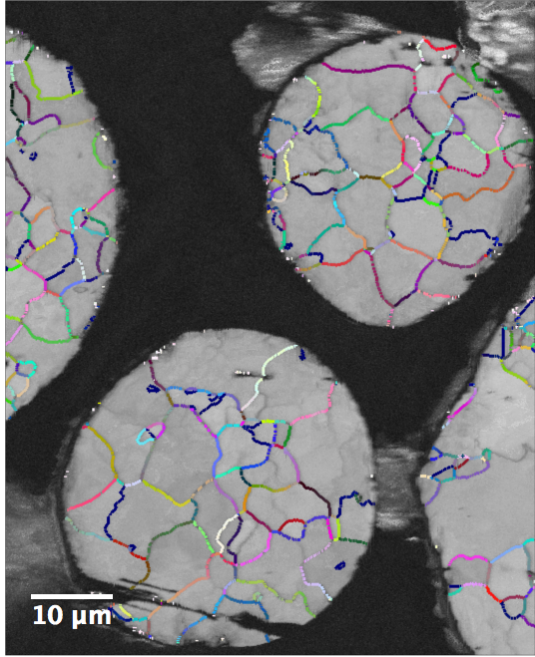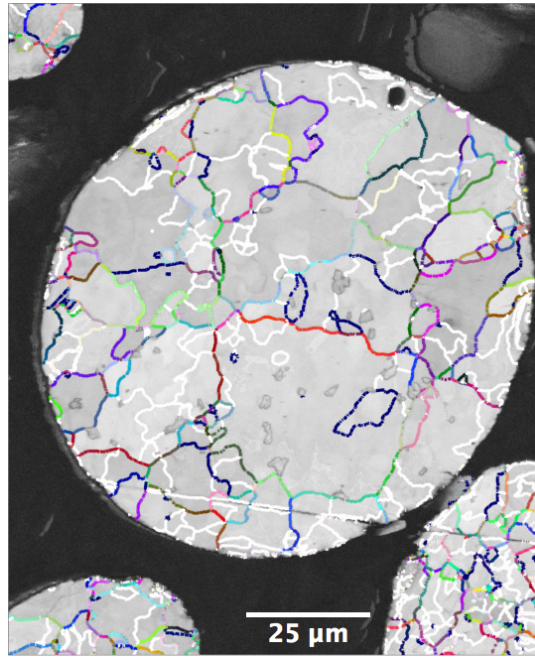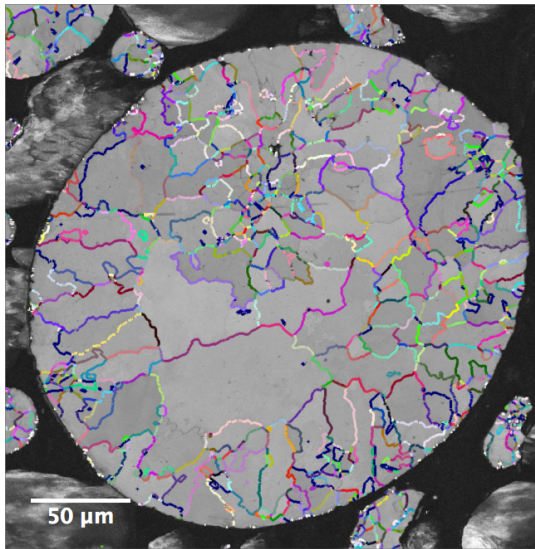
Figure 2: Grain boundary misorientation maps of as-received powder particles of different sizes (35 μm, 90 μm, and 225 μm) are shown in (a), (b), and (c). The grain boundaries are colour coded according to the legend shown in (e1). The legend is constructed using stereographic projection of surfaces of constant misorientation angle (ω) where each section is a standard stereographic triangle. The angle and axis information of any grain boundary can be obtained by matching its colour to the misorientation angle from the stereographic triangle and its position in the triangle, respectively. Only few sections are shown for illustration. Specific examples are shown in (e2), where the positions for $\Sigma 3$, $\Sigma 9$, and $\Sigma 27$ boundary colours are marked using circles on $60°$, $38.9°$, $31.6°$, and $35.4°$ misorientation surfaces. For a comparison, (c) is shown with only $\Sigma 3$, $\Sigma 9$, and $\Sigma 27$ boundaries highlighted (with a tolerance angle of $3°$ from ideal misorientation) in red, yellow, and blue, respectively in (d) (Colour online).

The fractions of $\Sigma 3^n$ boundaries (up to $n=2$) and triple junctions in the as-received powder are shown in Table 2; also shown are the statistics for the fully consolidated specimen for comparison. In the powder, as expected, most of the triple junctions contain random boundaries with J_0 fraction being highest. The statistics for the fully consolidated specimen, on the other hand, show an increased fraction of $\Sigma 3^n$ boundaries. However, most of the $\Sigma 3$ boundaries are part of J_1. Comparing the microstructures and the statistics for the powder and the fully consolidated specimen (Fig. 2, Fig. 3, and Tab. 2), it is clear that the microstructure changed from the one containing random boundaries in the as-received powder to a twin dominated one in the fully consolidated specimen. In order to understand this change, microstructures representative of those present at various stages during HIPing, were analyzed.

8
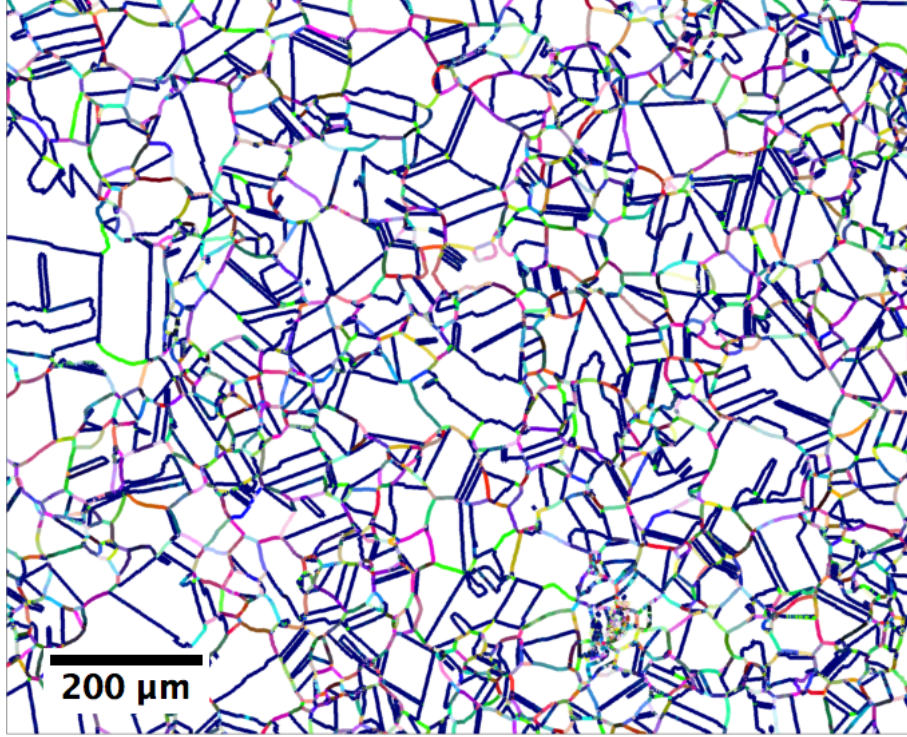
Figure 3: Grain boundary misorientation map of the fully consolidated 316L austenitic stainless steel specimen. Grain boundaries are colour coded according to the legend shown in Fig. 2e (Colour online).

Table 2: CSL boundary fractions and triple junction distributions averaged from the data of the three powder particles shown in Fig. 3, and for the fully consolidated specimen. Values in the brackets indicate standard deviation.

Sample	$\Sigma 3$		$\Sigma 9$		$\Sigma 27$		Total CSL ($\Sigma \leq 29$)		J_0	J_1	J_2	J_3
	L[†]	N[‡]	L	N	L	N	L	N				
Powder	8 (±1.5)	4 (±1)	<1	<1	<1	<1	14 (±1.9)	7 (±1)	80 (±5)	19 (±4)	<1	<1
FC*	53 (±1)	26 (±1.2)	1.56 (±0.1)	3 (±0.15)	0.7 (±0.1)	1 (±0.1)	60 (±1.5)	32 (±1.4)	25 (±2)	60 (±1)	6 (±0.6)	9 (±0.7)

[†]Length fraction.

[‡]Number fraction.

*Fully consolidated.

(a) 950 °C

(b) 1000 °C

(c) 1050 °C

(d) 1120 °C
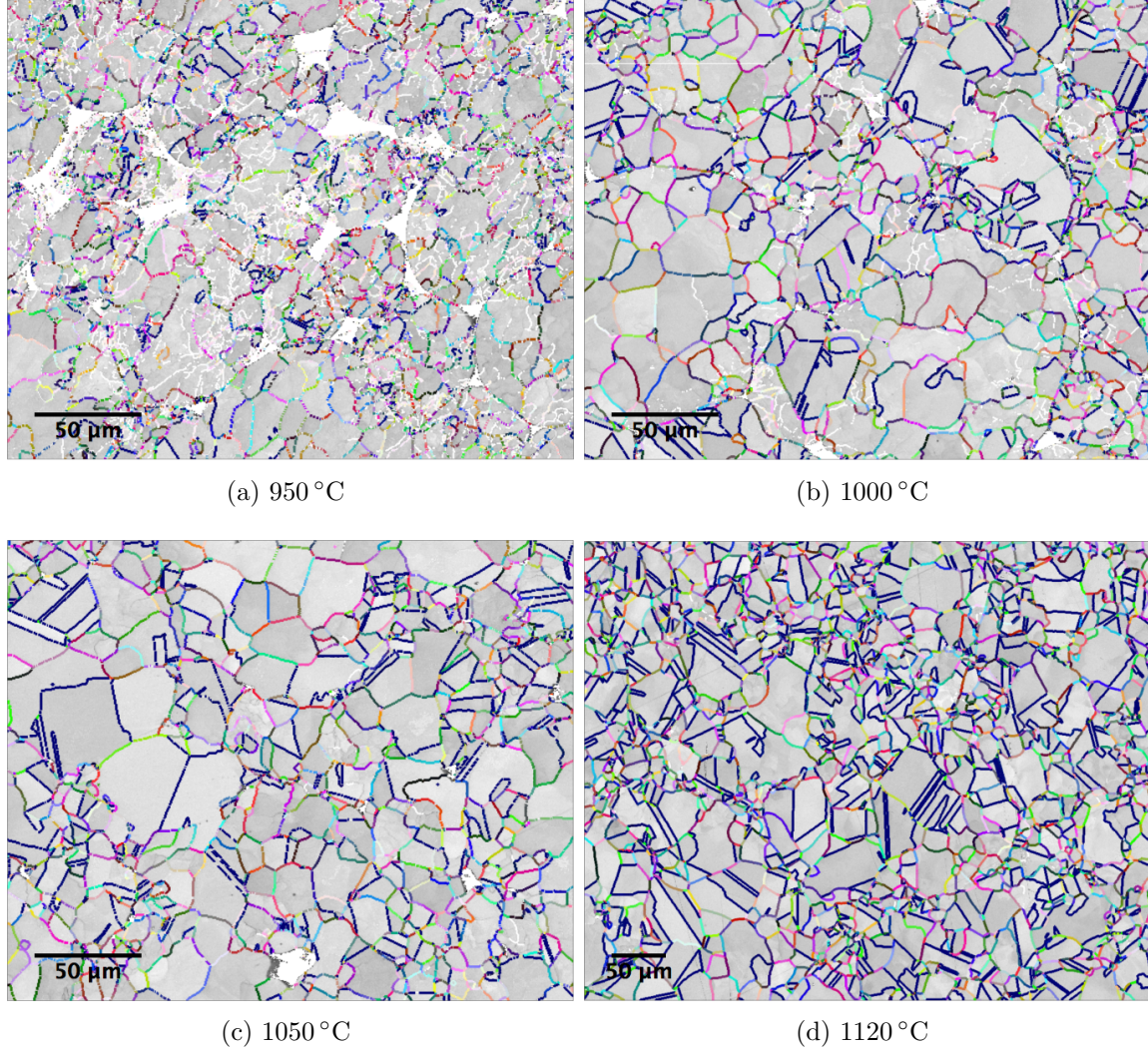
Figure 4: Grain boundary misorientation maps of 316L HIPed at a pressure of 103 MPa and at increasing temperatures, starting at 950 °C. The grain boundaries are colour coded according to the legend shown in Fig. 2e. The fraction of subgrain boundaries, shown in white colour, gradually decreases with concomitant increase in the fraction of annealing twins as the HIPing temperature increases (Colour online).
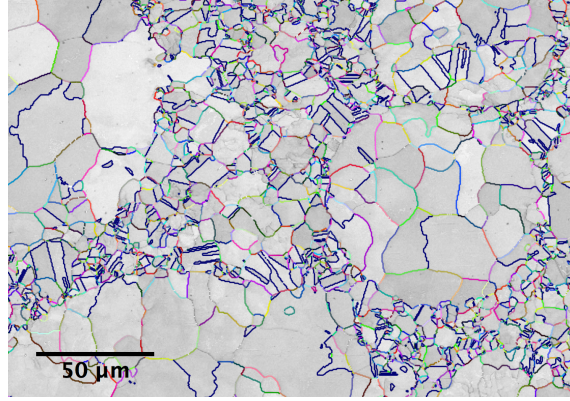
(a)

Figure 5: Grain boundary misorientation map of the sample HIPed at 1050 °C. The grain boundaries are colour coded according to the legend shown in Fig. 2e (Colour online).

(a)

(b)
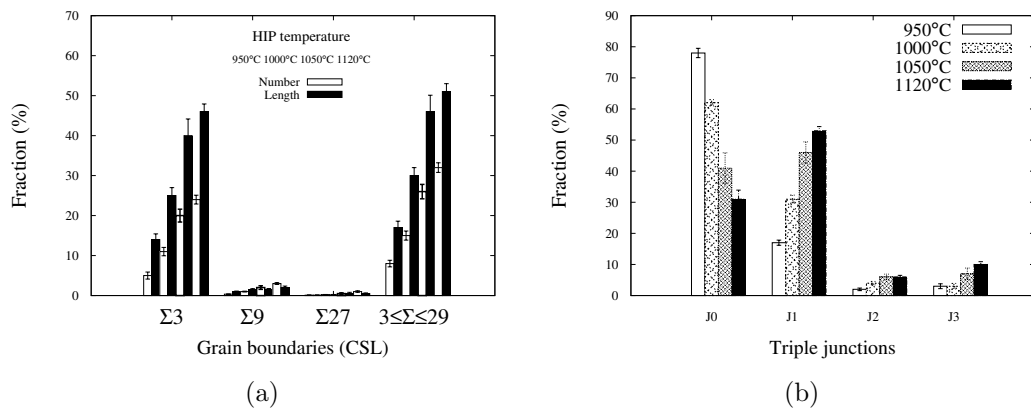
Figure 6: Evolution of (a) CSL boundary number and length fractions and (b) triple junction distribution as a function of HIPing temperature.

Representative grain boundary misorientation maps of partially consolidated HIPed samples are shown in Fig. 4. Extensive formation of subgrain boundaries, as a consequence of the incipient deformation of the powder particles, is seen in the sample HIPed at 950 °C (Fig. 4a). Along with porosity, powder particles are also clearly seen because of incomplete consolidation. In the sample HIPed at 1000 °C, incipient formation of annealing twins (qualitatively, seen as parallel sided boundaries; also see the legend for $\Sigma 3$ boundary in Fig. 2e.) is seen along with the presence of fewer subgrain boundaries (Fig. 4b) as compared to the sample HIPed at 950 °C. A decrease in the fraction of subgrain boundaries along with concomitant increase in the fraction of annealing twins is seen in the sample HIPed at 1050 °C (Fig. 4c). Further increase in the annealing twin fraction and a decrease in subgrain boundaries is seen in the sample HIPed at 1120 °C (Fig. 4d). Moreover, in certain regions of the partially consolidated samples, it was observed that smaller particles deformed more than larger particles; a representative misorientation map is shown in Fig. 5. Here, it is seen that annealing twins have formed profusely in smaller particles that are decorated around larger, non-deformed particles. It is also seen that the non-deformed particles have retained their identity (i.e., shape and grain boundary characteristics) of the as-received state (see Fig. 2).

Annealing twins that are formed during HIPing interact and form either higher order twins or a $\Sigma 1$ boundary (i.e., form $\Sigma 3^n$ boundaries; n can be 0 or >1; see [28]). As a result, the triple junctions with twin boundaries also evolve during HIPing. The evolution of number and length fractions of $\Sigma 3$, $\Sigma 9$, and $\Sigma 27$ and other *special* boundaries identified using the CSL theory framework (CSL ≤ 29), and the distribution of triple junctions (i.e., J_0, J_1, J_2, and J_3) as a function of HIPing temperature are shown in Fig. 6. As seen in Fig. 6a, there is an increase, both in number and length fractions, in the CSL boundaries, with the increase in HIPing temperature.

Fig. 6b shows distribution of triple junction types as a function of HIPing temperature. Triple junctions containing subgrain boundaries were not considered in the analysis. A decrease in the fraction of J_0 and increase in the fractions of other triple junctions is seen as the HIPing temperature is increased. The changes are more apparent for J_0, J_1, and J_3 fractions while the variation in J_2 with HIPing temperature is less pronounced. These observations are in accord with the increase in the fraction of $\Sigma 3^n$ boundaries as a function of HIPing temperature (Fig. 6a). In other words, as the fraction of twin boundaries (i.e., $\Sigma 3$, $\Sigma 9$, and $\Sigma 27$) increases, so will the fraction of triple junctions containing them.

During the early stages of HIPing, particles are deformed by the application of pressure at high temperature (i.e., they plastically yield), resulting in the formation of dislocations in the deformed particles. Since the deformation is at high temperature, the defect microstructure is simultaneously annealed. Formation of twin boundaries during
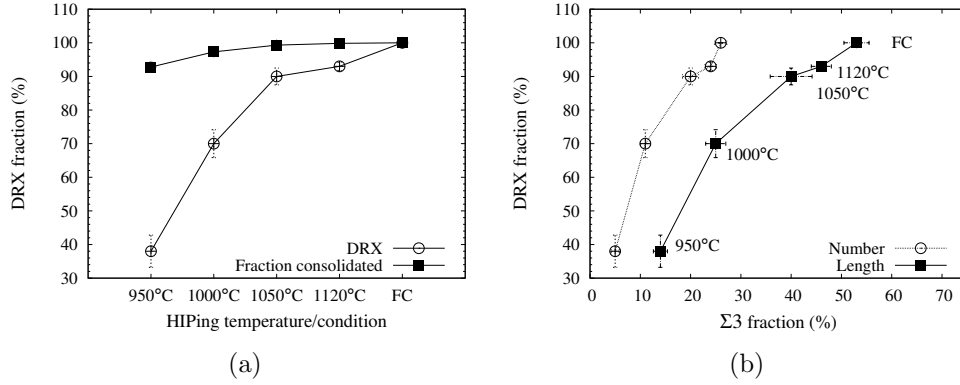
Figure 7: Evolution of (a) fractions recrystallized and consolidated as a function of HIPing temperature and (b) recrystallized fraction as a function of the $\Sigma 3$ fraction (FC: Fully consolidated). Lines joining the data points in (a) are only a guide to the eye.

high temperature deformation of the particles and a gradual increment in their fraction at progressively increasing temperatures (Fig. 4, and Fig. 6a) indicates the occurrence of dynamic recrystallization (DRX). In order to understand the progression of DRX, a criterion based on grain orientation spread (GOS[1]) was applied on the EBSD data of the specimens at each HIPing condition. A value for GOS (measured in degrees) which can differentiate the recrystallized grains from the deformed grains was obtained from the EBSD data of three different heats of fully consolidated and solution annealed samples (i.e., which are fully recrystallized). Any threshold value between $1°$ and $2°$ gave similar results in all specimens, with more than 99% of the area seen as recrystallized. However, sensitivity analysis on partially consolidated specimens revealed that the recrystallized fraction changed with the threshold value used. Specifically, with a change in the threshold value from $1.5°$ to $2°$, recrystallized fractions differed by about 20% for the samples HIPed at $950\,°C$ and $1000\,°C$, while the same for $1050\,°C$ and $1120\,°C$ samples, it was less than 4%. However, the change in recrystallized fraction was much larger for a change in the threshold value from $1°$ to $1.5°$. So, a $1.5°$ threshold for GOS was used for obtaining the DRX fractions in the partially HIPed specimens.

Fig. 7a shows the evolution of DRX and consolidated fractions obtained using EBSD data and image analysis, respectively, as a function of HIPing temperature. The consolidated fraction (or porosity fraction) from the optical images of the specimens at each HIPing condition was estimated using ImageJ software [44]. Due to the contrast difference between pores and the bulk specimen in the optical images, thresholding to obtain binary images was straightforward. It is seen that the DRX fraction increases with the HIPing temperature. For the specimen HIPed at $1120\,°C$, though little to no porosity was

---

[1]GOS is defined as "the average difference in orientation between the average grain orientation and all measurements within a single grain" [43].

observed in the microstructure (in other words, the specimen was nearly consolidated), it did not undergo complete recrystallization (i.e., it was ∼93% recrystallized). This suggests that the dwell time of 4 hours employed during the HIPing cycle (which is part of a standard HIPing cycle) further promotes recrystallization. This result is in accord with the evolution of DRX fraction as a function of annealing twins, which is shown in Fig. 7b. From the state where the specimen is HIPed at 1120 °C (no dwell time) to fully consolidated condition, annealing twins are still formed. This can be seen from the increase in their number fraction, i.e., from 23% to 26% (Fig. 6b). Also, the evolution of DRX fraction follows the number fraction of annealing twins at different HIPing temperatures (i.e., DRX fraction increases with the increase in the twin fraction), which suggests that during HIPing, this material recrystallizes by twinning.
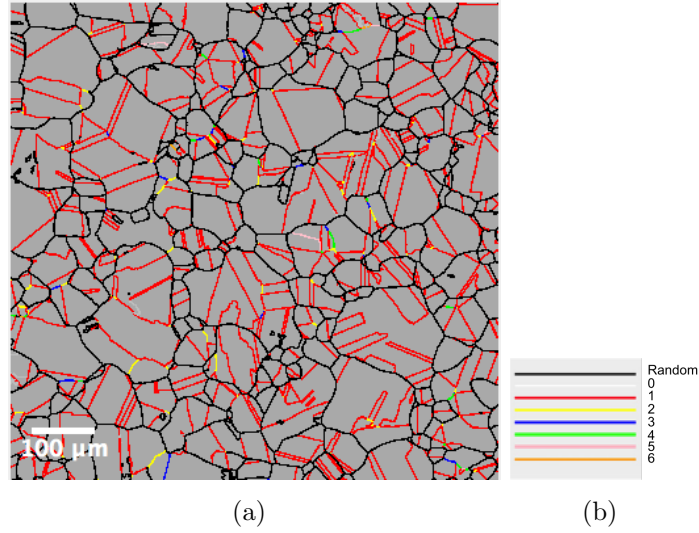
Figure 8: Twin related domains (TRDs) in fully consolidated specimen is shown in (a). The boundaries are coloured according to the legend shown in (b), where the numbers indicate n in $\Sigma 3^n$. The average number of grains in the TRDs was 3.77 while the average size of TRDs was 35 μm (Colour online).

TRDs, which are linked to recrystallization, were reconstructed for the fully consolidated specimen, and are shown in Fig. 8a with $\Sigma 3^n$ boundaries depicted as per the legend shown in Fig. 8b. A visual inspection of the map reveals the sizes of TRDs which, following the previous proposition [23, 33], can be treated as the classical grain size, and the random boundaries that highlight the paths along which cracks propagate. For the partially HIPed specimens, along with the TRD reconstruction, additional TRD parameters were also obtained; these are shown in Tab. 3. The average values of all TRD parameters increase as the HIPing process progresses. Specifically, for the specimen HIPed at 950 °C, $\langle N_g \rangle$ is close to 1, with $\langle LLC \rangle$=0.08; this means that most of the grains have not yet twinned (in other words, they have not recrystallized). This result can be correlated with low fractions of twin boundaries (see Fig. 6a). In the fully consol-

idated specimen, which has completely recrystallized, average values of TRD parameters have increased compared to the sample HIPed at 950 °C. Interestingly, albeit the sample is nearly consolidated by 1120 °C (without dwell time at that temperature), $\langle N_g \rangle$ and $\langle LLC \rangle$ values have increased after HIPing at 1160 °C (i.e., full HIP cycle); additionally, LLC_{max} has increased from 7 to 9 after the full HIPing cycle. This clearly shows that the sample recrystallizes during the 4 hour dwell time (in other words, twin chains in TRDs have propagated further), and is in agreement with the results shown in in Fig. 7. Increase in the $\langle TRD \rangle$ size from 14.2 μm to 35 μm indicates grain growth during the dwell time of HIPing cycle.

Table 3: $\langle TRD \rangle$, $\langle N_g \rangle$, $\langle LLC \rangle$, LLC_{max}, $\langle p \rangle$, and p_{max} for the specimens HIPed at different temperatures. Here, $\langle TRD \rangle$ is in μm while other parameters have no units.

HIPing temperature	$\langle TRD \rangle$	$\langle N_g \rangle$	$\langle LLC \rangle$	LLC_{max}	$\langle p \rangle$	p_{max}
950 °C	4.49	1.08	0.08	5	1.0	2.0
1000 °C	6.12	1.32	0.23	6	1.02	3.5
1050 °C	9.21	1.97	0.60	6	1.07	2.25
1120 °C	14.2	2.55	0.93	7	1.14	2.8
1160 °C	35	3.77	1.56	9	1.3	4.0

The frequency distributions for TRD size, N_g, and LLC for each HIPing condition, which effectively reflect their evolution during the HIPing process, are shown in Fig. 9. The TRD size distribution curves are seen to shift to the right as the function of HIPing temperature (Fig. 9a), resulting in an increase in the $\langle TRD \rangle$ size. A comparison between the average particle size of as-received powder and the average TRD size in fully consolidated specimen (80 μm and 35 μm, respectively) suggests that the length scale of TRDs will be less than the particle size. The disribution of LLC is shown in Fig. 9b. Not only does the LLC_{max} increase (also see Tab. 3), but the number of TRDs with LLC >0 also increases. Specifically, in the specimen HIPed at 950 °C, less than 1% of TRDs have $LLC \geq 2$ (LLC_{max}=5), while for the completely consolidated specimen, 33% TRDs have $LLC \geq 2$ (LLC_{max}=9). Similar observations can be made for the disribution of N_g, shown in Fig. 9c.

4 Discussion

4.1 Microstructural evolution during HIPing

4.1.1 Evolution of CSL boundaries and triple junctions

Grain boundary misorientation maps (Fig. 2) and the frequency of CSL boundaries ($3 \leq \Sigma \leq 29$) in the powder shown in Tab. 2, which was averaged over 3 particles of different
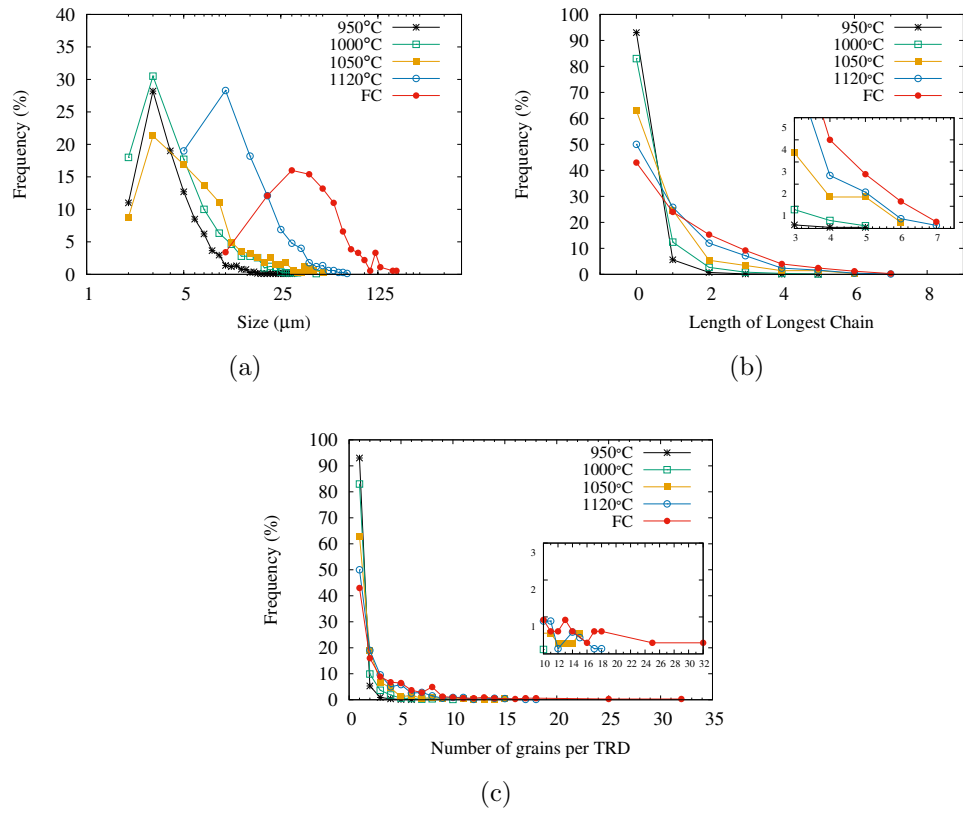
Figure 9: The distribution (a) TRD sizes (a) length of longest chain and (b) the number of grains in a TRD as a function of HIPing temperature; FC: fully consolidated (Colour online).

sizes, indicate that the microstructure is dominated by high angle grain boundaries. Most of the $\Sigma 3$ boundaries in the powder particles had deviations between 1 - 2° from the ideal misorientation. Since the grain boundary network is dominated by random high angle boundaries, the triple junctions observed in the powder were of J_0 type, followed by J_1, while very few J_2 and J_3 junctions were present (refer Tab. 2). During HIPing, a gradual increase in the twin fraction (first and higher order twins) is observed, as seen in the grain boundary misorientation maps (Fig. 4), and from the quantitative analysis of the EBSD data (Fig. 6a). In regards to the number and length fractions of twin boundaries (i.e., f_Σ^n and f_Σ^l, respectively, of $\Sigma 3$, $\Sigma 9$, and $\Sigma 27$) in the fully consolidated specimen, it is seen that $f_{\Sigma 3}^n < f_{\Sigma 3}^l$, $f_{\Sigma 9}^n > f_{\Sigma 9}^l$, and $f_{\Sigma 27}^n > f_{\Sigma 27}^l$. Since the majority of CSL boundaries consists of $\Sigma 3$, $f_\Sigma^n < f_\Sigma^l$ (see Tab. 2). Such differences between length and number fractions in CSL boundaries have previously been reported in the literature [22, 45, 21, 20].

Since the $\Sigma 3$ boundaries are straight and long (i.e., annealing twins), they are, on average, longer than other high angle grain boundaries, thus giving rise to the observed inequality (i.e., for $\Sigma 3$ and total CSL fraction) [21]. It has been suggested that the constraint imposed by the crystallography of the triple junctions necessitates the presence of $\Sigma 9$ and $\Sigma 27$ boundaries in the microstructure and that they have no energetic preference among other non-$\Sigma 3$ CSL boundaries for their nucleation [46] (relatively very few $\Sigma 9$ and $\Sigma 27$ boundaries were observed at J_1 in this study). Since the length per boundary of such *crystallographically necessary* boundaries at the triple junctions containing $\Sigma 3$ boundaries is often very small, it translates to f_Σ^n being greater than f_Σ^l for $\Sigma 9$ and $\Sigma 27$ boundaries.

The distribution of triple junctions has also evolved accordingly (Fig. 6b). Specifically, a decrease in the fraction of J_0 and an increase in the fraction of J_1, J_2, and J_3 junctions is seen, which correlates well with the increase in the number fraction of twin boundaries. Experimental results on the microstructural characterization of several low to medium SFE energy FCC materials have clearly demonstrated the non-random nature of the distribution of triple junctions, and have shown that it is related to the crystallographic constraints imposed at the triple junction [22, 24, 25, 47]. Specifically, if ΣA, ΣB, and ΣC are the grain boundaries meeting at the triple junction, then Σ-product rule dictates that the following relation be satisfied [28]:

$$\Sigma A \Sigma B = m^2 \Sigma C \tag{1}$$

where m is a common divisor of A and B. Eq. 1 further suggests that a triple junction will most likely contain a low-CSL boundary if the other two are Σ boundaries. In other words, the Σ-product rule constrains the grain boundary connectivity and in turn necessitates the presence of certain grain boundaries at the triple junctions. More specifically, as previously noted, in FCC materials which undergo profuse annealing twinning, the presence of higher fractions of $\Sigma 9$ and $\Sigma 27$ boundaries compared to other CSL bound-

aries is purely for crystallographic reasons (i.e., to satisfy Eq: 1) and not because of the energetics [46]. A geometric representation of Eq. 1 was given in Fig. 9 of [31], and for the specific case of twinning, it becomes $\Sigma 3^n . \Sigma 3^m = \Sigma 3^{n+m-2i}$, where i is an integer between 0 and n. If the Σ-combination rule is not enforced at the triple junctions, then their distribution as a function of CSL boundary fraction can be obtained using a general analytical probability function [48]:

$$P(i, f_\Sigma^n) = (-i^2 + 3i + 1)(f_\Sigma^n)^i (1 - f_\Sigma^n)^{3-i} \tag{2}$$

where $P(i, f_\Sigma^n)$ is the probability of having a triple junction with i CSL boundaries for a particular value of f_Σ^n in the microstructure (So, for $i = 0$, $P(i, f_\Sigma^n)$ gives the probability for J_0 for a given f_Σ^n, and so on).
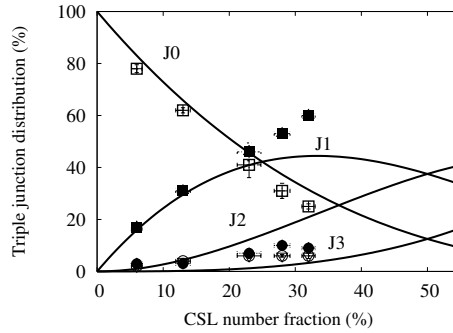

Figure 10: The triple junction distribution as a function of the fraction of *special* boundaries. The solid lines represent the solutions to the analytical probability functions without the combination rule enforced at the junctions [48]. The experimentally determined fractions are represented by J_0: □, J_1: ■, J_2: ○, J_3: ●.

Fig. 10 shows the plot of experimentally observed triple junctions in this study as a function of CSL boundary fractions along with the solutions of Eq: 2 for *i=1, 2, and 3*. It is seen that experimentally observed J_0 agrees well with the analytical probability distribution while the agreement is poor for other triple junctions, in accord with the observations of Kumar et al [22]. Since all boundaries at J_0 are *random*, the combination rule (i.e., Eq: 1) does not apply and the agreement with Eq: 2 is good. However, experimentally observed J_1 and J_3 fractions are higher than the analytical solutions while J_2 fraction is lower. Such a trend has previously been observed in a Ni-based alloy and Cu, which were thermomechanically processed to contain different fractions of CSL boundaries [22]. The results were rationalized on the basis of Eq. 1 and it was concluded that low-CSL boundaries more likely assemble at J_1 and J_3 junctions and less likely at J_2. Minich et al [47] and Schuh et al [24], by imposing crystallographic constraints at triple junctions in their models, successfully captured the experimentally observed trends in triple junction distribution as a function of *special* boundary fraction.

18

Results from the present study are in general agreement with their model (refer Fig. 3 in [24]).

4.1.2 Dynamic recrystallization and the development of TRDs during HIPing

In materials with low to medium SFE, elevated temperature deformation results in DRX [49, 50]. In these materials, it has been shown that the formation of high-order twin chains in single and polycrystals is a key feature of the recrystallized microstructure, and that twinning is an active nucleation mechanism for recrystallization [23, 51, 52, 53, 54, 55]. Although the present investigation was not aimed towards providing any additional insights on DRX, already established mechanism, i.e., twinning during DRX, is observed during HIPing of 316L powder.

The fraction recrystallized as a function of HIPing temperature was estimated using GOS criterion (Fig. 7a). It must however be noted that this fraction, which is around 38% for the specimen HIPed at 950 °C, also includes regions that have not undergone DRX. Specifically, regions within large particles, or particles themselves, that have features of the as-received state (in other words, they have not undergone deformation), yet having GOS <1.5° were observed. While in principle these regions have not recrystallized, they were treated to be part of the DRX region since their GOS value is <1.5°. This overestimation in DRX fraction decreases with increasing HIPing temperatures as most of the particles would have already deformed, and hence would have either recrystallized, or be in the deformed state. This, however, is dependent on the particle size distribution and applied pressure, as will be discussed in the next section.

In regards to recrystallization during HIPing, an important observation can be made from Fig. 7 and Tab. 3. The pressure used for HIPing the powder at different temperatures (i.e., 103 MPa) is high enough for them to plastically yield. Plastic deformation of the particles is only possible during early stages of HIPing (i.e., at 950 °C and 1000 °C in this study), where contact stresses between the particles are high, and is the main factor contributing to the densification. Once there are isolated pores, creep, grain boundary and bulk diffusion contribute to densification. Therefore, the stored energy due to the plastic deformation of particles at early stages contributes to recrystallization at higher temperatures; this is because, there is little porosity at higher temperatures for the compact to deform as most of the densification has already happened. It is then the case of static recrystallization (SRX) and/or strain induced boundary migration (SIBM) contributing to microstructural changes during final stages of HIPing (i.e, after 1050 °C and during dwell time). In other words, during HIPing, the microstructure evolves via dynamic and static recrystallization. However, distinction has not been made in the present study.

19

It is observed that the propagation of twin chains during HIPing, as seen from the evolution of $\langle LLC \rangle$ and LLC_{max}, makes the specimen more polysynthetic (refer Tab. 3). In other words, during HIPing process, as the specimen recrystallizes, reverse twinning is promoted. Lind et al [27] analyzed TRDs in 3D using near-field high-energy diffraction microscopy (nf-HEDM) on a synchrotron source in a normal and a grain boundary engineered copper sample, respectively, and demonstrated that grain boundary engineered sample is more polysynthetic than the normal sample. Liu et al [56], in a grain boundary engineered nickel based alloy, have demonstrated that multiple twinning results in the formation of back and forth pattern (in other words, both higher and lower generations of twin orientations are produced). However, a strong preference for reverse twinning (i.e., polysynthetism) and hence, certain orientations was observed. It thus appears that multiple twinning, regardless of the processing condition, results in the material becoming more polysynthetic.

4.2 Factors influencing the development of grain boundary network in HIPed 316L steels

Size dependent inhomogenous nature of plastic deformation of particles is an important aspect during HIPing, which affects the final microstructure. Specifically, Fig. 5 clearly demonstrates that smaller particles deform more than larger particles. This result is in accord with the ones reported in other investigations [57, 58, 59, 60], and can be rationalized based on the fact that the fraction of contact area to the available surface area is higher for smaller particles than for larger particles. As illustrated by Wright et al in their HIP model, small particles will see increased deformation if present in interstices of an arrangement of large particles [61]. In addition, the mechanical properties of the powder particles vary depending on their size. Specifically, if we consider two different powder sizes shown in Fig. 2 (i.e., 35 μm and 225 μm) and their average grain size, the larger particle contains an order of magniture more number of grains than the smaller particle. Consequently, in general, larger particles would be harder than smaller particles because they contain many more grains that constrain each other during deformation. So, even with the theoretical density achieved after a full HIPing cycle, depending on the particle size distribution, some non-deformed particles can still remain in the compact. In other words, they would just retain their original shape, and won't undergo recrystallization; this is illustrated in Fig. 11a. It shows the reconstructed TRDs for a region in a fully consolidated specimen that has not completely recrystallized (i.e., a powder particle is partially in its original state). The region surrounding the particle has recrystallized, as evidenced by the presence of annealing twins. In order to see if the as-received powder when annealed at high temperature undergoes recrystallization, it was

put in a capillary and heat treated at 1100 °C for 15 minutes under argon atmosphere. Comparing the grain boundary network of the heat treated powder (shown in Fig. 11b) with that of non-deformed region in the fully consolidated specimen (Fig. 11a), it is seen that they are very similar. This further suggests that the as-received powder does not have enough stored energy for it to recrystallize if it has not deformed, albeit subjected to full HIPing cycle.

So, it can be understood that a temperature cycle without simultaneous (or prior) deformation of the particles would only result in grain boundary migration and perhaps grain growth, and that deformation of the particles is a prerequisite for recrystallization (compare Fig. 11b with the as-received powder shown in Fig. 2). It must be noted that this is not a universal feature of gas-atomized powders; it has recently been demonstrated that powders of titanium aluminide undergo recrystallization even with a simple heat treatment without prior plastic deformation [62]. Specifically, Guyon et al have shown that the elastic coherency strain and interfacial energy in the particles provide the driving force for recrystallization even in the absence of prior plastic deformation [62].

| (a) | (b) | (c) |
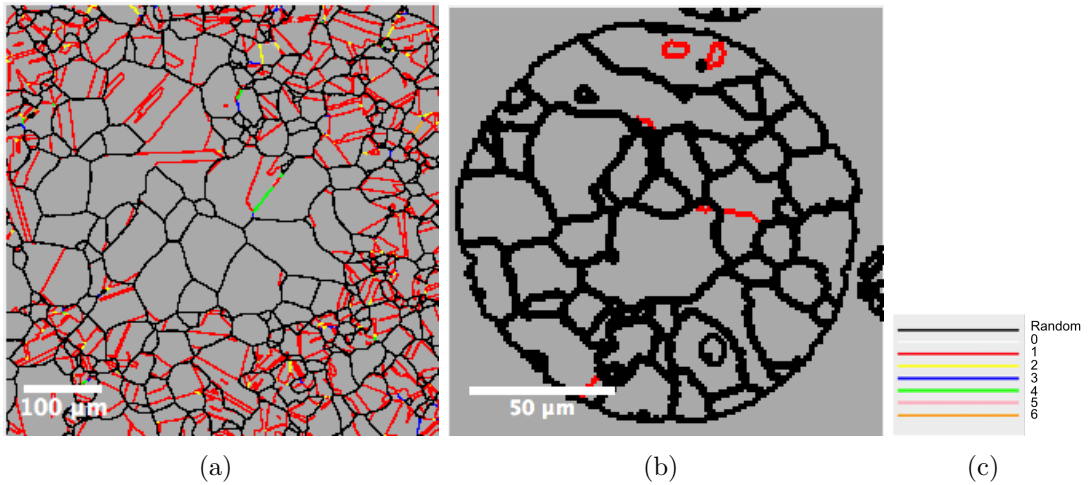
Figure 11: (a) TRDs in a region in the completely consolidated specimen, which contains a powder particle that has not deformed. The peripheral region of the particle and the region surrounding the particle have recrystallized, amounting to a rigid particle sitting in a soft matrix. Further deformation is not possible as the compact has been completely consolidated. TRDs in a heat treated powder particle are shown in (b). Similarity between the two (i.e., a and b) confirms that particles need to undergo deformation to recrystallize. Legend is shown in (c), where the numbers indicate n in $\Sigma 3^n$ (Colour online).

While the tendency of a material to twin depends primarily on the chemistry (in other words, SFE), thermomechanical processing has a second order, but strong, effect (e.g., [45] and references therein). Similar to the case where the grain boundary networks in low to medium SFE materials produced from solidification route strongly depend on their

thermomechanical processing history, grain boundary network of HIPed 316L depends strongly on particle characteristics and processing parameters. Liu et al [34] have studied the effect of initial grain size on the development of grain boundary network during grain boundary engineering (GBE) of alloy 690. Besides showing the effect of pre-strain level on the recrystallized microstructure, it was also demonstrated that a large initial grain size increases the TRD size but reduces the twin boundary density, and a small initial grain size induces higher twin boundary density, but higher random boundary density and smaller TRD size. This in principle applies to HIPed 316L. Here, the size distribution of powder particles, their grain size, the extent they are strained to, the temperature, and time, affect TRD development.

Specifically, the average grain size of the powder depends on the size of the powder; large particles have relativey larger grain size than the small particles (Fig. 2). The level of strain experienced by the particles depends on their packing fraction (in other words, their tap density), which in turn is governed by the particle characteristics (size distribution and morphology) and the applied pressure. Specifically, high packing fractions result in low shrinkage of the compact and therefore low strains, while low packing fractions result in high shrinkage and high strains. The importance of dwell time was highlighted previously. Specifically, it was observed that twin chains in the TRDs propagate further during the 4 hour dwell time of the HIPing cycle (see Tab. 3). With particle characteristics unaltered, the effect of decreasing or increasing the dwell time on final microstructure needs further investigation.

4.3 Possibilities of grain boundary control in NNS PM-HIPed components

Thermomechanical processing of cast materials allows the realization of a variety of microstructures and hence, a range of properties. For low to medium SFE materials (e.g., 316L, 304L, alloy 690), control of grain boundary network using various *strain-anneal* or *strain-recrystallization* processes that result in $\Sigma 3$ and high-order twin boundaries to be part of the grain boundary network has been shown to improve their performance. However, in the case of powder-HIP manufacturing, only post-HIP heat treatments are possible if the principal objective is to achieve near net shape. Preceeding discussion on how the grain boundary network evolves during HIPing, and the factors affecting it, offers some potential directions that could be pursued to exercise control over the development of grain boundary network. Since these changes can be applied during the HIPing process, they can be implemented on near net shape components. Two examples are presented. It must be noted that the aim here is to only demonstrate that the topology of the grain boundary network can be changed by altering the traditionally used HIPing cycle; it is

an optimization problem and no attempts were made towards the same in the present study.
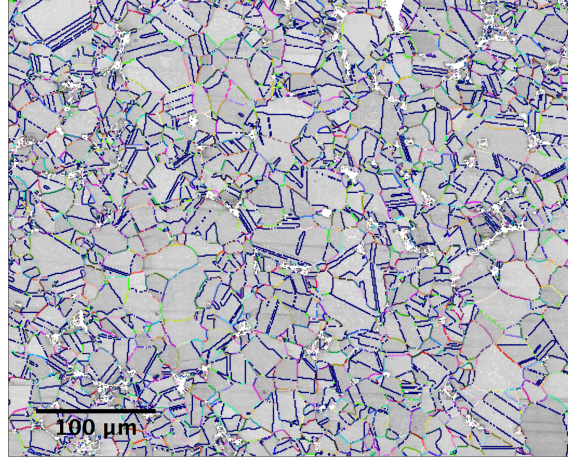

Figure 12: Grain boundary misorientation map of the specimen HIPed at 950 °C and subsequently heat treated at 1100 °C for 10 min. It had undergone static recrystallization as a result of the heat treatment. The grain boundaries are colour coded according to the legend shown in Fig. 2e (Colour online).

Fig. 12 shows the grain boundary misorientation map of the sample HIPed at 950 °C (without any dwell time), which was subsequently annealed for 10 min at 1100 °C (i.e., post-HIP). A comparison with the microstructure of 950 °C as-HIPed specimen (see Fig. 4a) reveals that the heat treated specimen has undergone static recrystallization (SRX). The fraction of twin boundaries and triple junction distribution in the annealed specimen was found to be similar to those of the specimen HIPed at 1120 °C. Quantitative analysis for the specimens, i.e., as-HIPed at 950 °C and its annealed condition are shown in Tab. 4 (950HIP and 950HIP+10mHT, respectively). A dramatic decrease in J_0, but an increase in J_1, J_2, and J_3 fractions is seen. This heat treatment is akin to the *strain-anneal* process used in GBE of low to medium SFE materials. Noting that the sample is still partially consolidated (some porosity is visible in Fig. 12), re-HIPing this sample would create some stored energy as a result of deformation of the powder particles. The heat treated sample, during re-HIPing, could either undergo further recrystallization or SIBM, potentially resulting in a change in the grain boundary network compared to the normally HIPed specimen. Recall that a single step *strain-anneal* process is a demonstrated method to increase the twin boundary fraction (and consequently, the TRD sizes) in 316L [36]. However, extension to HIPing requires process optimization, which should also take into account, the requirement of uniform dimensional changes during HIPing. In this regard, HIP modelling should prove helpful.

Another example is shown in Fig. 13. Here, the grain boundary misorientation map of a completely consolidated specimen that contains 95 ppm of oxygen is shown in Fig.

23
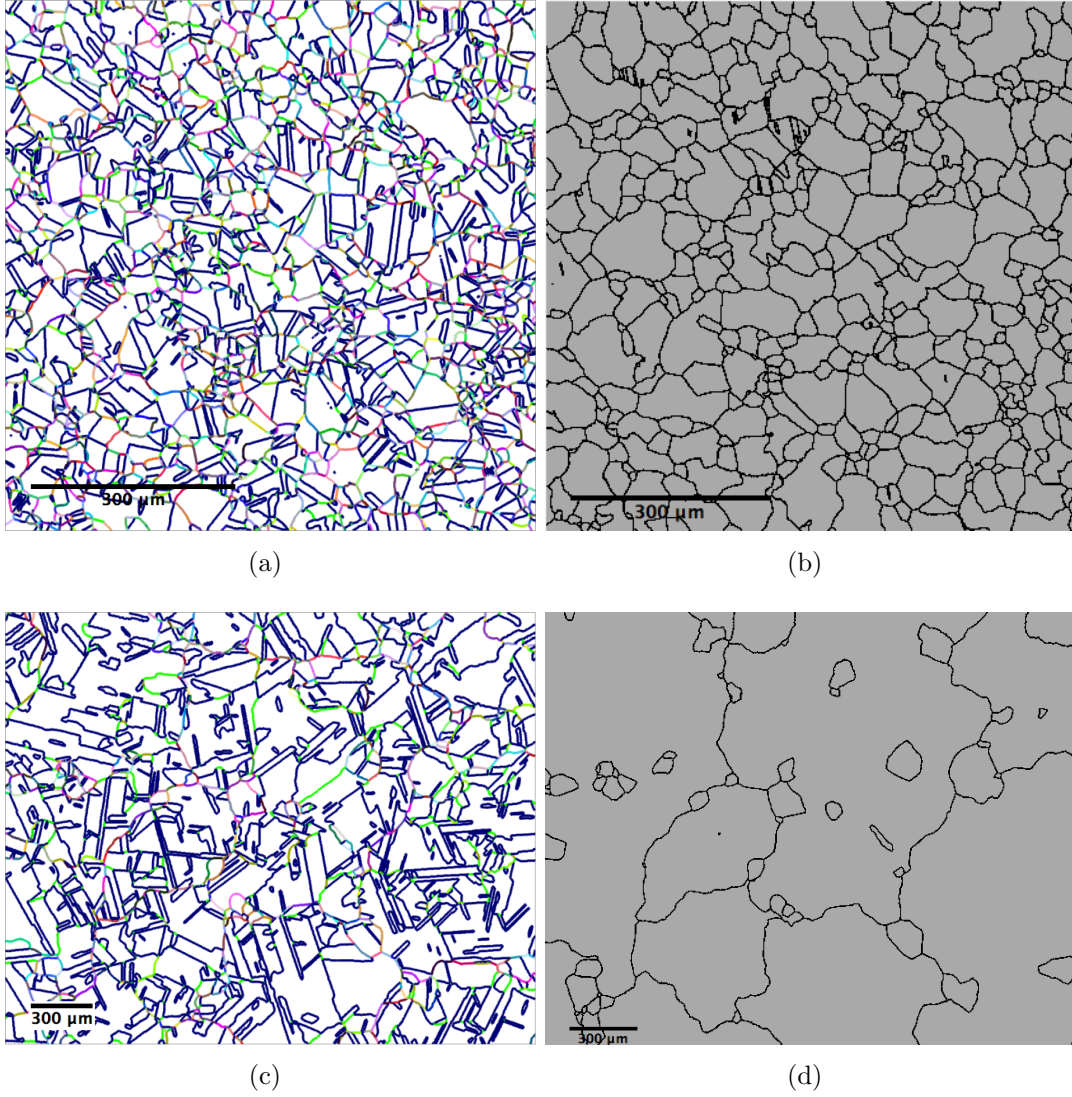
Figure 13: (a) Grain boundary misorientation map of a fully consolidated specimen with 95 ppm of oxygen. Parent grains of TRDs are shown in (b). Grain boundary misorientation map and parent grains of TRDs of the same specimen after annealing at 1100 °C for 66 hours are shown in (c) and (d), respectively. Changes in the grain boundary network are apparent. The grain boundaries in (a) and (c) are colour coded according to the legend shown in Fig. 2e (Colour online).

24

13a while the outer boundaries delineating the TRDs (i.e., parent grains) are shown in Fig. 13b. This specimen was subsequently annealed for 66 hours at 1100 °C. The misorientation map and TRD map of annealed specimen are shown in Fig. 13c and Fig. 13d, respectively. Two features are apparent. First, there is considerable grain gowth and second, the twin boundary fraction is much greater in the annealed specimen, which is inferred from the quantitative analysis of triple junction and TRD statistics, shown in Tab. 4 (FC and FC+66hrHT, respectively). Change in the grain boundary network is perhaps due to the boundary migration driven by residual strains present in the specimen. Similar heat treatment on the sample with higher oxygen content did not result in such dramatic change indicating that oxygen, which is mainly in the form of oxide inclusions, has a strong influence on the grain coarsening/grain boundary migration during post-HIP annealing. As is the case with previous example, along with oxygen control, post-HIP heat treatments need to be optimized (e.g., shorter time at lower temperature).

Table 4: A comparison of triple junction distributions and the average TRD parameters for four specimens, highlighting the effect of heat treatments.

Sample	J_0	J_1	J_2	J_3	$\langle TRD \rangle$	$\langle N_g \rangle$	$\langle LLC \rangle$	LLC_{max}	$\langle p \rangle$	p_{max}
950HIP	78	17	2	3	4.49	1.08	0.08	5	1.0	2.0
950HIP+10mHT	38	46	5	11	15	2.51	1	8	1.13	2.75
FC	15	59	8	18	31	4.2	1.57	8	1.3	3.33
FC+66hrHT	1	45	4	50	156	16.81	2.13	9	1.57	6.12

Another important observation can be made from Tab. 4; the statistics for FC specimen with 95 ppm of oxygen (see the metrics for FC in Tab. 4) and completely consolidated specimen with 200 ppm oxygen (see the final row in Tab. 2 and Tab. 3) are different in that the extent of multiple twinning is more in the former. This again shows the influence of particle characteristics and chemistry on the development of grain boundary network. The two examples shown above, demonstrate that there is a potential for controlling the grain boundary network in HIPed samples even in the case where imparting NNS to the component is the main objective.

5   Conclusions

The aim of the present study was to understand the evolution of grain boundary network in 316L austenitic steel during HIPing. The main findings are:

- The as-received nitrogen gas atomized powder predominantly contained a network of random boundaries while the completely consolidated HIPed material had a large

25

fraction of annealing twins, indicating that the principal mechanism governing the microstructural evolution during HIPing is recrystallization (DRX and SRX).

- As-received powder does not have enough stored energy to recrystallize without deformation. Plastic deformation of the particles, which occurs at high temperature during early stages of HIPing, is a prerequisite for recrystallization. Because of the size dependence on the extent of their deformation, particle size distribution strongly influences the final microstructure.

- The recrystallized fraction increases during both ramping up stage (i.e., of P and T) as well as during the dwell time of the HIPing cycle, and correlates well with the evolution of number fraction of $\Sigma 3$ boundaries. While the fraction of triple junctions containing $\Sigma 3$ boundaries increases concomitantly, they are predominantly part of J_1 triple junctions.

- Quantitative analysis of TRDs, which are linked to recrystallization, reveals that $\langle TRD \rangle$, $\langle N_g \rangle$, $\langle LLC \rangle$, and $\langle p \rangle$ increase during HIPing.

- By altering the particle characteristics, HIPing cycle, and post-HIP heat treatments, it is possible to change the grain boundary network, indicating the potential for grain boundary engineering during HIPing.

Finally, it must be recognized that HIPing is a thermomechanical process. While in most cases, the primary objective of powder based HIPing is to produce a fully dense component, of significant importance is the microstructural evolution during HIPing and the topology of the grain boundary network in the fully consolidated material. Powder characteristics (particle size distribution, grain size, morphology, tap density, chemistry etc), the HIPing cycle, and post-HIPing heat treatment have a critical role to play in the development of the final microstructure. For materials which profusely twin (e.g., 316L, alloy 600 and 690), even with the constraints imposed by the way in which pressure and temperature can be applied, HIPing process can potentially be tailored to produce increased fractions of twin boudaries that are part of the grain boudary network. Such an optimized process is of great value because of the added benefit of the component being of near net shape.

Acknowledgements

References

[1] H. V Atkinson and S. Davies. Fundamental aspects of hot isostatic pressing: an overview. *Metallurgical and Materials Transactions A*, 31A(December):2981–3000, 2000.

[2] S. J. Zinkle and G. S. Was. Materials challenges in nuclear energy. *Acta Materialia*, 61(3):735–758, 2013.

[3] D. Gandy, J. Siefert, L. Lherbier, and Novotnak. D. PM-HIP Research for Pressure Retaining Applications Within the Electric Power Industry. In *ASME 2014 Small Modular Reactors Symposium*, pages 1–13, Washington, 2014.

[4] B. W. Burdett, P. Hurrell, and A. Gilleland. Hot isostatic pressing of austenitic stainless steel powders for pressure retaining applications. In *ASME/JSME 2004 Pressure Vessels and Piping Conference*, pages 153–160. American Society of Mechanical Engineers, 2004.

[5] J. L. Sulley, I. Hookham, B. Burdett, and K. Bridger. Introduction of Hot Isostatically Pressed, Reactor Coolant System Components in PWR Plant. In *18th International Conference on Nuclear Engineering*, pages 357–367. American Society of Mechanical Engineers, 2010.

[6] J. L. Sulley, B. K. Bull, and A. C. Wood. Hot isostatic pressing of large bore, stainless steel pipework for a safety critical application. In *Advanced Materials Research*, volume 378, pages 752–758. Trans Tech Publ, 2012.

[7] A. J. Cooper, N. I. Cooper, Bell. A, Dhers. J, and A. H. Sherry. A Microstructural Study on the Observed Differences in Charpy Impact Behavior Between Hot Isostatically Pressed and Forged 304L and 316L Austenitic Stainless Steel. *Metallurgical and Materials Transactions A*, 46(11):5126–5138, 2015.

[8] A. J. Cooper, N. I. Cooper, Dhers. J, and A. H. Sherry. Effect of Oxygen Content Upon the Microstructural and Mechanical Properties of Type 316L Austenitic Stainless Steel Manufactured by Hot Isostatic Pressing. *Metallurgical and Materials Transactions A*, 47(9):4467–4475, 2016.

[9] J. P. Hirth. The influence of grain boundaries on mechanical properties. *Metallurgical Transactions*, 3(12):3047–3067, 1972.

[10] G. A. Chadwick and D. A. Smith. *Grain boundary structure and properties*. Academic Press, 1976.

27

[11] R. Z. Valiev, V. Yu. Gertsman, and O. A. Kaibyshev. Grain boundary structure and properties under external influences. *Physica status solidi (a)*, 97(1):11–56, 1986.

[12] D. Wolf and S. Yip. *Materials Interfaces: Atomic-level Structure and Properties.* Springer Science & Business Media, 1992.

[13] A. P. Sutton and R. W. Balluffi. Interfaces in crystalline materials (monographs on the physics and chemistry of materials. 2007.

[14] H. Grimmer, W. Bollmann, and D. H. Warrington. Coincidence-site lattices and complete pattern-shift in cubic crystals. *Acta Crystallographica Section A*, 30(2):197–207, Mar 1974.

[15] E. A. Trillo and L. E. Murr. A TEM investigation of $M_{23}C_6$ carbide precipitation behaviour on varying grain boundary misorientations in 304 stainless steels. *Journal of Materials Science*, 33(5):1263–1271, 1998.

[16] H. U. Hong, B. S. Rho, and S. W. Nam. Correlation of the $M_{23}C_6$ precipitation morphology with grain boundary characteristics in austenitic stainless steel. *Materials Science and Engineering: A*, 318(1–2):285 – 292, 2001.

[17] D. C. Crawford and G. S. Was. The role of grain boundary misorientation in intergranular cracking of Ni-16Cr-9Fe in 360 C Argon and high-purity water. *Metallurgical Transactions A*, 23(4):1195–1206, 1992.

[18] E. M. Lehockey, Palumbo. G, Lin. P, and A. M. Brennenstuhl. On the relationship between grain boundary character distribution and intergranular corrosion. *Scripta Materialia*, 36(10):1211–1218, 1997.

[19] V. Y. Gertsman and S. M. Bruemmer. Study of grain boundary character along intergranular stress corrosion crack paths in austenitic alloys. *Acta Materialia*, 49(9):1589–1598, 2001.

[20] S. Bechtle, M. Kumar, B.P. Somerday, M.E. Launey, and R.O. Ritchie. Grain-boundary engineering markedly reduces susceptibility to intergranular hydrogen embrittlement in metallic materials. *Acta Materialia*, 57(14):4148 – 4157, 2009.

[21] C. A. Schuh, M. Kumar, and W. E. King. Universal features of grain boundary networks in FCC materials. *Journal of Materials Science*, 40(4):847–852, 2005.

[22] M. Kumar, A. J. Schwartz, and W. E. King. Microstructural evolution during grain boundary engineering of low to medium stacking fault energy fcc materials. *Acta Materialia*, 50(10):2599 – 2612, 2002.

[23] V. Y. Gertsman and C. H. Henager. Grain boundary junctions in microstructure generated by multiple twinning. *Interface Science*, 11(4):403–415, 2003.

[24] C. A. Schuh, R. W. Minich, and M. Kumar. Connectivity and percolation in simulated grain-boundary networks. *Philosophical Magazine*, 83(6):711–726, 2003.

[25] C. A. Schuh, M. Kumar, and W. E. King. Analysis of grain boundary networks and their evolution during grain boundary engineering. *Acta Materialia*, 51:687–700, 2003.

[26] D. L. Engelberg, R. C. Newman, and T. J. Marrow. Effect of thermomechanical process history on grain boundary control in an austenitic stainless steel. *Scripta Materialia*, 59(5):554 – 557, 2008.

[27] J. Lind, S. F Li, and M. Kumar. Twin related domains in 3D microstructures of conventionally processed and grain boundary engineered materials. *Acta Materialia*, 114:43–53, 2016.

[28] K. Miyazawa, Y. Iwasaki, K. Ito, and Y. Ishida. Combination rule of Σ values at triple junctions in cubic polycrystals. *Acta Crystallographica Section A: Foundations of Crystallography*, 52(6):787–796, 1996.

[29] V. Y. Gertsman. Geometrical theory of triple junctions of CSL boundaries. *Acta Crystallographica Section A: Foundations of Crystallography*, 57(4):369–377, 2001.

[30] W. R. Bryan and M. Kumar. Mathematical methods for analyzing highly-twinned grain boundary networks. *Scripta Materialia*, 54(6):1029 – 1033, 2006. Viewpoint set no. 40: Grain boundary engineering.

[31] C. Cayron. Multiple twinning in cubic crystals: Geometric/algebraic study and its application for the identification of the $\Sigma 3^n$ grain boundaries. *Acta Crystallographica Section A: Foundations of Crystallography*, 63(1):11–29, 2007.

[32] S. Xia, B. Zhou, and W. Chen. Grain cluster microstructure and grain boundary character distribution in alloy 690. *Metallurgical and Materials Transactions A*, 40(12):3016–3030, 2009.

[33] C. Cayron. Quantification of multiple twinning in face centred cubic materials. *Acta Materialia*, 59(1):252–262, 2011.

[34] T. Liu, S. Xia, B. Zhou, Q. Bai, C. Su, and Z. Cai. Effect of initial grain sizes on the grain boundary network during grain boundary engineering in alloy 690. *Journal of Materials Research*, 28(09):1165–1176, 2013.

[35] X. Fang, Z. Liu, M. Tikhonova, A. Belyakov, and W. Wang. Evolution of texture and development of $\Sigma 3^n$ grain clusters in 316 austenitic stainless steel during thermal mechanical processing. *Journal of Materials Science*, 48(3):997–1004, 2013.

[36] M. Michiuchi, H. Kokawa, Z. J. Wang, Y. S. Sato, and K. Sakai. Twin-induced grain boundary engineering for 316 austenitic stainless steel. *Acta Materialia*, 54:5179–5184, 2006.

[37] M. Shimada, H. Kokawa, Z. J. Wang, Y. S. Sato, and I. Karibe. Optimization of grain boundary character distribution for intergranular corrosion resistant 304 stainless steel by twin- induced grain boundary engineering. *Acta Materialia*, 50:2331–2341, 2002.

[38] B. W. Reed, R. W. Minich, R. E. Rudd, and M. Kumar. The structure of the cubic coincident site lattice rotation group. *Acta Crystallographica Section A*, 60(3):263–277, May 2004.

[39] R. Hielscher and H. Schaeben. A novel pole figure inversion method: specification of the *MTEX* algorithm. *J. Appl. Crystallogr.*, 41(6):1024–1037, Dec 2008.

[40] C. Cayron. *ARPGE*: a computer program to automatically reconstruct the parent grains from electron backscatter diffraction data. *Journal of Applied Crystallography*, 40(6):1183–1188, Dec 2007.

[41] S. Patala and C. A. Schuh. A continuous and one-to-one coloring scheme for misorientations. *Acta Materialia*, 59(2):554–562, 2011.

[42] S. Patala, J. K. Mason, and C. A. Schuh. Improved representations of misorientation information for grain boundary science and engineering. *Progress in Materials Science*, 57(8):1383–1425, 2012.

[43] D. P. Field, L. T. Bradford, M. M. Nowell, and T. M. Lillo. The role of annealing twins during recrystallization of cu. *Acta materialia*, 55(12):4233–4241, 2007.

[44] C. A. Schneider, W. S. Rasband, and K. W. Eliceiri. NIH Image to ImageJ: 25 years of image analysis. *Nat Meth*, 9(7):671–675, 2012.

[45] V. Randle. Twinning-related grain boundary engineering. *Acta Materialia*, 52(14):4067–4081, 2004.

[46] V. Yu. Gertsman and Tangri. K. A study of grain boundary statistics in 304 and 316L stainless steels. *Philosophical Magazine A*, 64(6):1319–1330, 1991.

[47] R. Minich, C. Schuh, and M. Kumar. Role of topological constraints on the statistical properties of grain boundary networks. *Physical Review B*, 66(5):1–4, 2002.

[48] P. Fortier, W. A. Miller, and K. T. Aust. Triple junction and grain boundary character distributions in metallic materials. *Acta materialia*, 45(8):3459–3467, 1997.

[49] R. W. CAHN. {CHAPTER} 28 - {RECOVERY} {AND} {RECRYSTALLIZATION}. In R. W. CAHN and P. HAASEN†, editors, *Physical Metallurgy (Fourth, Revised and Enhanced Edition)*, pages 2399 – 2500. North-Holland, Oxford, fourth, revised and enhanced edition edition, 1996.

[50] A. Rollett, F. J. Humphreys, G. S. Rohrer, and M. Hatherly. *Recrystallization and related annealing phenomena*. Elsevier, 2004.

[51] S. Hoekstra, J. W. H. G. Slakhorst, and J. Huber. The development of recrystallization textures in (110) [001] and (110)[112] ag single crystals after a plane-strain deformation of 80.9 *Acta Metallurgica*, 25(4):395 – 406, 1977.

[52] P. J. Wilbrandt and P. Haasen. HVEM of the recrystallization of tensile deformed ⟨110⟩-oriented copper single crystals. *Zeitschrift fur Metallkunde*, 71(6):385–395, 1980.

[53] P.-J. Wilbrandt. The limits of a reliable interpretation of recrystallization texture in terms of multiple twinning. *physica status solidi (a)*, 61(2):411–418, 1980.

[54] G. Gottstein. Annealing texture development by multiple twinning in f.c.c. crystals. *Acta Metallurgica*, 32(7):1117 – 1138, 1984.

[55] X. Wang, E. Brünger, and G. Gottstein. The role of twinning during dynamic recrystallization in alloy 800 H. *Scripta Materialia*, 46(12):875–880, 2002.

[56] T. Liu, S. Xia, B. Wang, Q. Bai, B. Zhou, and C. Su. Grain orientation statistics of grain-clusters and the propensity of multiple-twinning during grain boundary engineering. *Materials & Design*, 112:442–448, 2016.

[57] S. V. Nair and J. K. Tien. Densification mechanism maps for hot isostatic pressing (HIP) of unequal sized particles. *Metallurgical Transactions A*, 18(1):97–107, 1987.

[58] W. A. Kaysser, M. Aslan, E. Arzt, M. Mitkov, and G. Petzow. Microstructural Development and Densification During Hipping of Ceramics and Metals. *Powder Metallurgy*, 31(1):63–69, 1988.

[59] E. K. H. Li and P. D. Funkenbusch. Hot isostatic pressing (hip) of powder mixtures and composites: Packing, densification, and microstructural effects. *Metallurgical Transactions A*, 24(6):1345–1354, 1993.

[60] H. R. Piehler and D. P. Delo. Physical modeling of powder consolidation processes. *Progress in Materials Science*, 42(1-4):263–276, 1997.

[61] R. N. Wright, R. L. Williamson, and J. R. Knibloe. Modelling of Hipping Consolidation Applied to Ni$_3$Al Powders. *Powder Metallurgy*, 33(3):253–259, 1990.

[62] J. Guyon, A. Hazotte, F. Wagner, and E. Bouzy. Recrystallization of coherent nanolamellar structures in Ti48Al2Cr2Nb intermetallic alloy. *Acta Materialia*, 103:672–680, 2016.